Preparation, Structural, and Dielectric Properties of (1-x)Pb(Zr$_{0.52}$Ti$_{0.48}$)O$_3$–x BiFeO$_3$ Composites

Malika Ahabboud[1],*, Najwa Gouitaa[1], Fatimazahra Ahjyaje[1], Taj-dine Lamcharfi[1], Farid Abdi[1], Mustapha Haddad[2]

* malikasmp2013@gmail.com

[1] Signals, Systems and Components Laboratory (LSSC), Electrical Engineering Department, University Sidi Mohamed Ben Abdellah, Faculty of Sciences and Technologies, Fez, Imouzzer Road B.P. 2202, Morocco
[2] Spectrometry, Materials and Archaeomaterials Laboratory (LASMAR), Faculty of Sciences, Moulay Ismail University, Meknes, Morocco

Abstract: *In this paper, we reported the preparation and characterization of (1-x)PbZr$_{0.52}$Ti$_{0.48}$O$_3$-xBiFeO$_3$ (1-x)PZTxBFO (x= 0.00, 0.15, 0.30, 0.45, 0.60 and 1.00) ceramics which prepared by sol-gel process for PZT and hydrothermal reaction for BiFeO$_3$ (BFO). The perovskite structure of the studied composite was detected by X-ray diffraction and Raman spectroscopy, while the microstructure images were characterized by scanning electron microscopy (SEM). Rietveld analysis confirmed the coexistence of these three phases; rhombohedral (R3m) and tetragonal phases (P4mm) for pure PbZr$_{0.52}$Ti$_{0.48}$O$_3$ (PZT) and only the rhombohedral structure (R3c) for pure BFO. Raman spectroscopy of the (1-x)PZT-xBFO composites showed two clear bands around 150 and 180 cm^{-1} and the intensities of Raman modes decreased with BFO concentration increased. Scanning electron microscope (SEM) analysis revealed that, as the BFO level increased, the grains in the materials became larger and denser. Additionally, the BFO sample produced a larger grain size than the other composites. The Energy-dispersive X-ray spectroscopy (EDS) spectra indicated that all the characteristic lines of the chemical elements Pb, Zr, Ti, and O and Bi, Fe, and O are present for the PZT and BFO materials respectively. The temperature-dependent dielectric constant shows the presence of the phase transition at frequencies below 1 MGh and the resonance phenomenon at frequencies above 1 MHz, in addition to a new phenomenon at x= 0.15. Indeed, the dielectric properties improved with an increase in dopant concentration of BFO in PZT, and novel dielectric resonance phenomena were found.*

Keywords: Multiferroic ceramics, Composites, EDS analysis, Dielectric resonance.

1. INTRODUCTION

Multiferroic materials are defined by the coexistence of two or more ferroic orders, such as ferroelectric, ferromagnetic, or ferroelastic phases coexist [1, 2]. These materials, which exhibit ferroelectric and magnetic order have attracted considerable interest due to their potential applications such as random access memory, spintronic sensors, spin filters, transducers, actuators, high-frequency filters, multi-state memories, resonators, etc [2, 3–6]. The Multiferroics have electric polarization and generate magnetization proportionate to the external magnetic field and external electric field respectively, and the coexistence of ferro-order and piezo-elastic properties can engender interesting piezo-electric and piezo-magnetic couplings [7, 8].

Ceramics present enormous attention for their technological applications because the coupling between the ferro-phases and the piezo-elastic properties improves a direct control of ferroelectric and ferromagnetic properties via externally applied mechanical stress [9, 10]. Among these classes of materials, Bismuth ferrite BiFeO$_3$ (BFO) is one of the rare single-phase multiferroic materials that present concurrently, at room temperature, ferroelectric and specific ferromagnetic orders. It has been extensively studied as a consequence of its high antiferromagnetic Neel temperature (T$_N$= 370°C) and ferroelectric Curie temperature (T$_C$= 830°C) [11–13]. The BFO with rhombohedral perovskite structure (space group R3c) is difficult to achieve, as secondary phases specifically Bi$_2$O$_3$, Bi$_2$Fe$_4$O$_9$, Bi$_{25}$FeO$_{40,}$ and Bi$_{25}$FeO$_{39}$ continually appear due to the kinetics of the structure formation [14–16]. However, The creation of Bi-O-Bi bridges between the non-bridging structural hydroxyl groups in the solution was caused by the increased concentration of KOH utilized in the process [17]. Thus, the dissolved Bi^{3+} hydroxides formed Bi$_2$O$_3$ crystallites, and the absorbed Fe^{3+} ions on Bi$_2$O$_3$

particles diffused into insolvable Bi_2O_3 and then produced precipitations of $Bi_2Fe_4O_9$ and $Bi_{25}FeO_{40}$ [18]. So, the secondary phases and irregular grains were detected in XRD patterns and SEM images for specimens synthesized with a high KOH concentration of up to 10 M and a low temperature of about 160°C [19].

On the other hand, Lead zirconate titanate $Pb(Zr_{1-x}Ti_x) O_3$ (PZT) is among the most essential materials for piezoelectric and ferroelectric applications. The PZT is defined as a solid solution of ferroelectric lead titanate $PbTiO_3$ (Tc= 490°C) and antiferroelectric lead zirconate $PbZrO_3$ (Tc= 230°C) with tetragonal and rhombohedral structures, respectively [20]. PZT phase diagram consists mainly of three regions at room temperature; The Zr-rich rhombohedral zone is divided from the Ti-rich tetragonal zone by a morphotropic phase boundary (MPB) in which the two structures coexist. This phase boundary is interesting due to its excellent piezo and dielectric properties [21, 22].

In this work, we synthesized pure perovskite phase PZT nano-crystalline by sol-gel method and BFO ceramics by hydrothermal process to obtain the $(1-x)PbZr_{0.52}Ti_{0.48}O_3-xBiFeO_3$ (PZT-BFO) multiferroic nanocomposites. In PZT-BFO composites, high doses of insulating PZT significantly increased the ferroelectricity and decreased the magnetization [7]. Compared with single-phase materials, ferromagnetic/ ferroelectric composites offer a different performance class with higher magneto-electric response coefficients [5, 8]. The structural and dielectric properties have been reported in the literature [23, 24]. Subhash Sharma and R.K. Dwivedi prepared the PZT-BFO ceramics using the sol-gel method and studied their structural, dielectric, and magnetic properties [25]. Vikash Singh et al found that X-ray diffraction data reveals the presence of tetragonal (P4mm) and monoclinic (Cm) phases for different compositions [26]. Chao Yan and al studied the ferroelectric and dielectric behaviors of the PZT-BFO composite. They confirmed that thanks to the presence of compressive stress, the Gibbs free energy has been flattened and the increase in the number of surfaces has intensified interfacial polarization [27]. So, this paper aims to present detailed structures and dielectric properties of this composite. The reason for studying the $(1-x)PZT-xCFO$ material is because coupling

ferroelectric PZT and ferromagnetic BFO has excellent dielectric and magnetic properties, as well as being used in a wide range of applications.

2. EXPERIMENTAL PROCEDURES

2.1. Materials

For experiments, the preparation of multiferroic nanocrystals is divided into three steps; 1) The PZT powders are firstly prepared by sol-gel method using $[PbC_2H_3O_2)_2.3H_2O]$, $[Zr(CH_3COO)_4]$ and $[Ti(OCH(CH_3)_2)_4]$ as starting precursors. These precursors are wet mixed, dried, and heat-treated at 700°C for 4 h to obtain the perovskite phase. The detailed preparation process is reported in other publications [28, 29]. Secondly, for BFO, we use the hydrothermal process and typical synthesis procedures are as follows; The iron nitrate $(Fe(NO_3)_3.9H_2O)$ and bismuth nitrate $(Bi(NO_3)_3.5H_2O)$ dissolved into distilled water and dilute nitric acid respectively. The two obtained solutions were mixed for about half an hour. Then, a solution of NaOH (8 M) was rapidly added to the above solution to jointly precipitate Bi^{3+} and Fe^{3+} ions, and a brown precipitate formed. This precipitate was filtered and washed with distilled water to remove $(NO_3)^-$ and Na^+ ions then dried at 80°C for 24 h. The resulting powder is ground and mixed with drops of NaOH solution and distilled water under stirring for 30 min. The powders were transferred into a Teflon-lined automatic autoclave of the bottom stirrer type for hydrothermal treatment at a temperature of 200° for 6 hours. After cooling to room temperature, the powders collected at the bottom of the Teflon liner were then filtered and washed with distilled water many times. Finally, the powders dried at 80°C for 24 h for characterizations. Finally, PZT and BFO powders were taken in different mole percent ratios according to the formula (1-x)PZT-xBFO with x= 0.00, 0.15, 0.30, 0.45, 0.60 and 1.00. All the compositions ground thoroughly and mixed in acetone for 4 hours. This dried mixture was followed by the addition of polyvinyl alcohol (PVA) as a binder to form pellets that sintered at 950° for 2 h. The pellets were carried out for characterization and measurements.

2.2. Equipment and Characterization

The structure and phase composition of the powders were investigated by X-ray diffraction

2

with Cu Kα radiation in a 2θ range of 15–80° at room temperature. X-ray diffraction data were analyzed via the Rietveld method using Fullprof software. Raman spectroscopy was measured at room temperature. The particle size and morphology were observed using scanning electron microscopy (SEM) and X-ray energy dispersive spectroscopy (EDS) is also studied. The dielectric properties of the (1-x)PZT-xBFO samples were carried out using an Agilent impedance analyzer (Agilent E4980A) in the frequency range from 100 Hz to 2 MHz and a wide range of temperatures (50–550°C).

3. RESULTS AND DISCUSSION

3.1. Structural Analysis

Figure 1 shows the X-ray diffraction (XRD) patterns of (1-x)PZT-x BFO ceramics. The results show characteristic peaks of PZT and BFO without any additional phases[30–32]. With the addition of BFO to PZT material, the structural nature of (1-x)PZT-x BFO remained unchanged. The quantity of the constituent phases determines the intensity of diffraction peaks. Consequently, as the amount of BFO increases, the intensity of peaks characteristic of the BFO phase increases, while the intensity of peaks characteristic of PZT decreases. This has been confirmed in the literature [26].
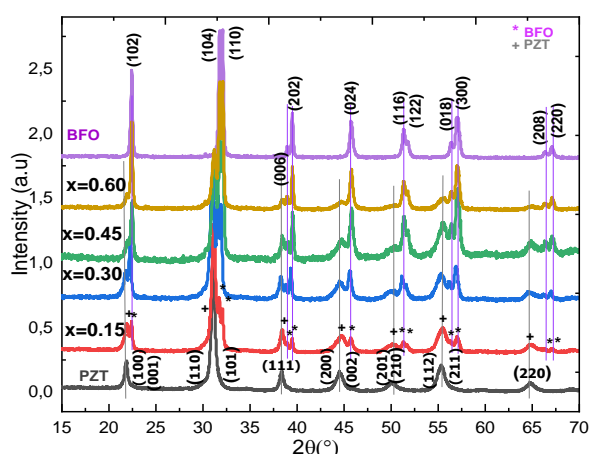

Fig. 1. XRD patterns of (1-x)PZT-xBFO composites

To obtain detailed structure parameters of (1-x)PZT-x BFO ceramics, Rietveld refinements were used to analyze the XRD data of the samples using FullProf software. The pseudo Voigt peak shape function option was chosen to define the peak profiles and the background was estimated

by linear interpolation between fixed values. Rietveld fitted diffraction patterns of all the studied samples are presented in Figure 2.

It has been observed that PZT ceramic (x= 0.00) shows a good fitting with goodness-of-fit parameter χ^2 close to 1 (table 1) and reveals two distinct phases; tetragonal and rhombohedral structures with spaces groups (P4mm) and (R3m) respectively. The coexistence of these two phases is due to the morphotropic phase boundary [33]. For x= 1.00, Rietveld analysis confirms the match of data observed with R3c space groups related to the rhombohedral phase. The same pure rhombohedral phase formation was found by C. Chen et al for BFO ceramic synthesis by hydrothermal route with KOH concentration 4 M and treatment temperature 220°C for 6 h [34]. While the obtained results for pure PZT and BFO are consistent with those reported in the literature [28, 35]. Similarly, for 0< x< 1 the refined data is found to be in good agreement with experimental data with the existence of three phases: tetragonal and rhombohedral phases (PZT phase) and rhombohedral phase (BFO phase). The factor R patterns Rp, Rwp, and the goodness-of-fit parameter χ^2 as well as the lattice parameters (a, b, c) for all the samples are given in Table 1. The lattice parameters are in good agreement with the literature [36]. This table shows a steady decrease in the lattice parameter ˋaˊˊ when concentration BFO increases from x= 0.15 to 0.45 for the rhombohedral phase of BFO. Above x= 0.45, this parameter increases for x= 0.60 and then decreases. This general decrease in the unit cell of the BFO sample is probably due to the Pb^{2+} with a large ionic radius (1.49 Å) substituting Bi^{3+} ions with a low ionic radius (1.30 Å). The particle sizes of all the powders, given in Table 1, present an anomaly at x= 0.30. Furthermore, the lattice parameters of both PZT structures are varied in fluctuation. These results can be attributed to site saturation due to the different ionic radii of ions: Bi^{3+} (1.30 Å) and Fe^{3+} (0.65 Å) more than Pb^{2+} (1.49 Å), Zr^{4+} (0.72 Å) and Ti^{4+} (0.68 Å) respectively.

To study the stability of the phase during sintering, we performed sintering of the 0.4PZT-0.6BFO composite pellet at different temperatures (900, 950, and 1000°C for 2 h). XRD patterns of the pellets are shown in Figure 3. From these results, we can confirm the formation of the phases corresponding to PZT and BFO

perovskites for all temperatures. But we can notice the appearance of a secondary peak attributed to Bi_2O_3 at $2\theta= 28°$ [37] for sintered samples at 900°C and 950°C, which is less intense at 950°C. At 1000°C, we observe an increase in the intensity of the Bi_2O_3 peak and the formation of other secondary peaks. Based on these results, we performed sintering of the (1-x)PZT-x BFO pellets at 950°C for 2 h.

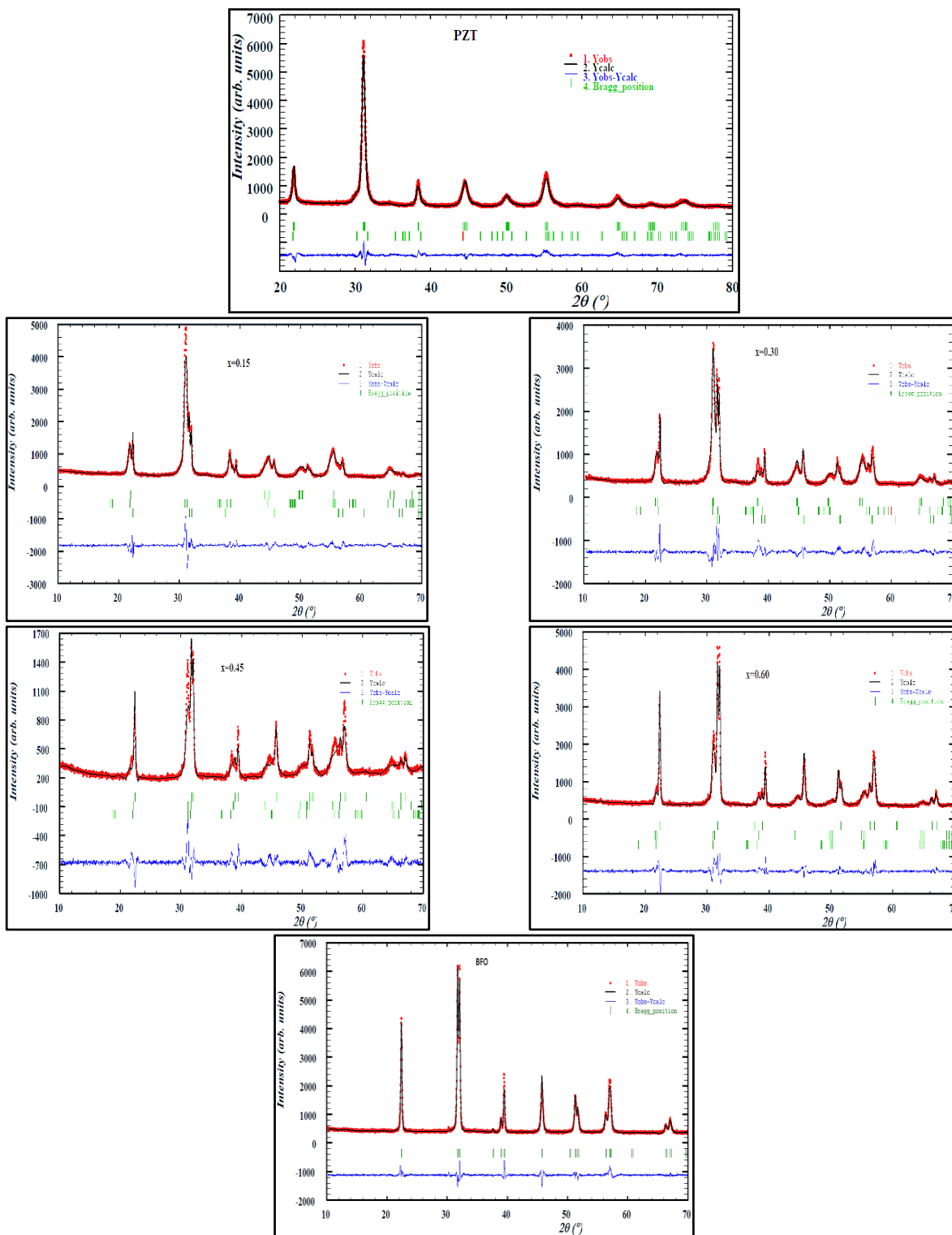**Fig. 2.** Rietveld refinement of (1-x)PZT-xBFO powders

Table 1. Refined structural parameters and particle sizes of (1-x)PZT-xBFO samples

x	Lattice constants (Å) and % phases			Factors χ^2 R_P, R_{wp}			Particle Sizes (nm)
	BFO (Rhm)	PZT (tetra)	PZT (Rhm)	χ^2	Rp (%)	Rwp	
x= 0.00	---------	a= 4.0402 c= 4.1098 48.42%	a= 5.7510 c= 14.1262 51.58%	1.12	3.92	4.97	17.83
x= 0.15	a= 5.5938 c= 13.8937 14.20%	a= 4.0418 c= 4.1076 82.81%	a= 5.7236 c= 14.2765 2.99%	2.94	6.11	8.13	12.62
x= 0.30	a= 5.5891 c= 13.8814 22.01%	a= 4.0568 c= 4.1083 13.45%	a= 5.6364 c= 14.3511 64.53%	3.55	6.47	8.95	8.17
x= 0.45	a= 5.5829 c= 13.8609 38.27%	a= 3.9935 c= 4.1311 59.13%	a= 5.6736 c= 14.1275 2.60%	2.82	6.99	9.51	8.64
x= 0.60	a= 5.5848 c= 13.8883 75.72%	a= 4.0537 c= 4.1042 10.41%	a= 5.7489 c= 14.1927 13.86%	2.66	5.50	7.35	11.06
x= 1.00	a= 5.5785 c= 13.8678 100%	---------	---------	1.87	4.70	6.22	14.83
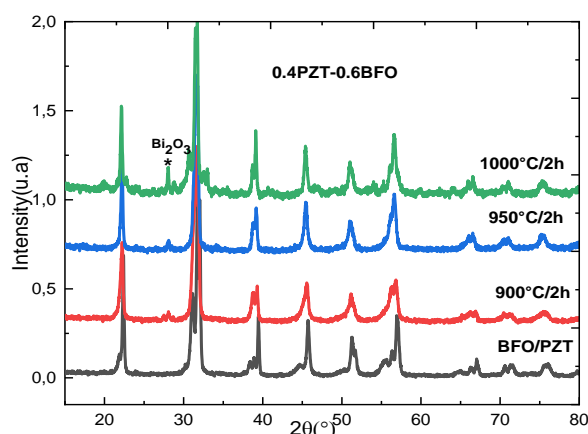
Fig. 3. X-ray diffractogram of 0.4PZT-0.6BFO powders sintered at different temperatures

3.2. Raman Spectroscopy

Figure 4 shows Raman spectra of (1-x)PZT-xBFO samples measured at room temperature. The Raman peaks of pure PZT and BFO materials are observed and identified with no additional peaks. These peaks are assigned using the studies done in the literature by Sharma and Yan [7, 26]. For pure PZT, the typical 3A1+B1+4E mode in the Raman peaks can be identified. The main peaks at 203, 274, 331, 507, 552, 597, 717, and 775 cm⁻¹, corresponding to the E(2TO), E+B1, A1(2TO), E(3TO), E(4TO), A1(3TO), E(4LO) and A1(3LO) modes respectively. Modes below 350 cm⁻¹ are attributed to distortion of TiO$_6$ octahedra. The modes in the range 350-610 cm⁻¹ correspond to

O-Ti-O bending and 610-850 cm⁻¹ correspond to Ti-O stretching [33, 38]. The characteristic bands of PZT are all in agreement with those found in previous studies [39, 40]. BFO exhibits distorted rhombohedral perovskite structure with the space group R3c. According to the group theory, 13 Raman modes are expected (4A1+9E). For our study, the pure BFO shows 9 active Raman modes out of the 13 modes reported in the R3c rhombohedral structure. For the (1-x)PZT-xBFO composites, two clear bands are visible around 150 and 180 cm⁻¹, but the intensity is much lower than for pure BFO. The stereochemical activity of the lone electron pairs of Bi and Pb plays the main role in the modification of two Bi-O covalent bonds into six characteristic modes E1, A1(1), A1(2), A1(3), A1(4) and E2 [41]. These modes are believed to be responsible for the ferroelectric nature of bismuth ferrite samples [42]. In addition, the typical strong modes corresponding to Bi-O covalent bond, A1(1), A1(2), and A1 (3) shift to a lower wavenumber with increasing BFO content compared to pure PZT. This can be attributed to the smaller atomic weight of Pb^{2+} (207.2) and Ti^{4+} (47.86) compared to Bi$^+$ (208.98) and Fe^{3+} (55.84). Furthermore, it is seen that the intensity of the A1(2TO) mode increases from x= 0.00 to x= 0.45 and then decreases may be due to the structural distortion of the materials. Then, the E(4LO) and A1(3LO) modes are eliminated for x= 0.60 and 1.00 samples.
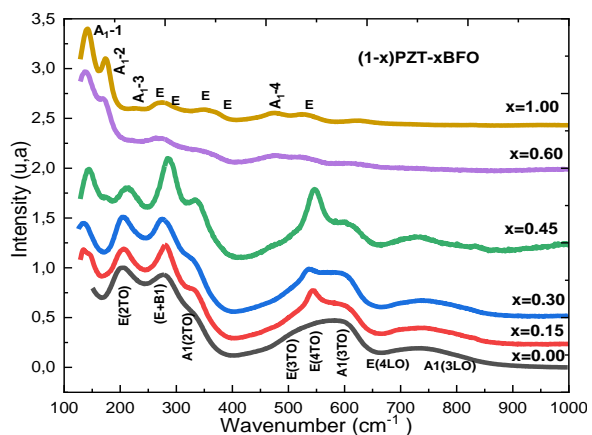
Fig. 4. Raman spectra of (1-x)PZT-x BFO powders

The disappearance of some peaks and a decrease in the intensity of the A1 modes confirm the transformation of the crystal structure with doping [41, 43].

3.3. SEM and EDS Analysis

The morphological analyses of the surface of (1-x)PZT-xBFO samples sintered at 950°C for 2 h are performed by scanning electron microscopy (SEM). The SEM images are shown in Figure 5. The images show that small grains with semi-spherical shapes begin to agglomerate and form into large complex clusters as BFO increases.
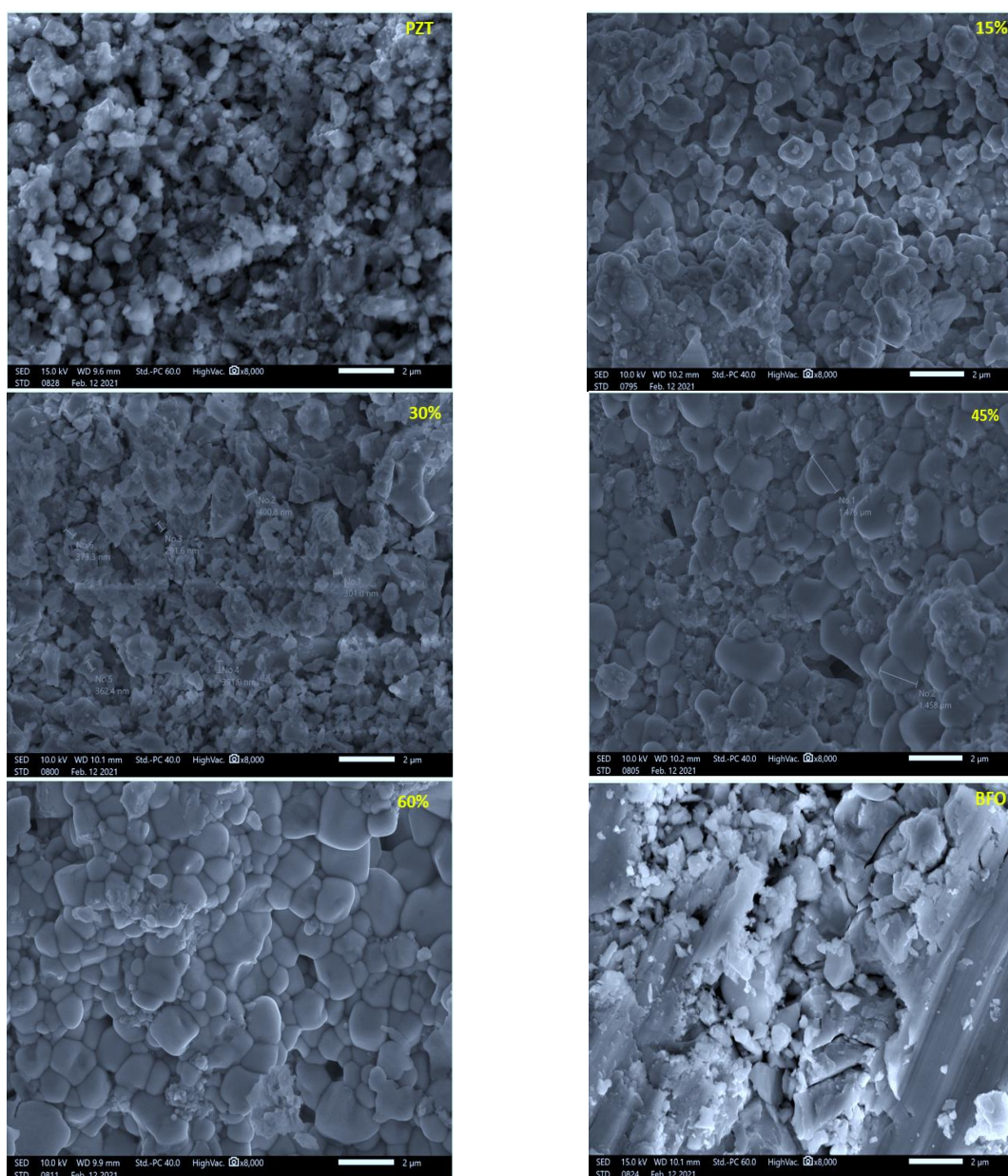

Fig. 5. SEM micrographs of (1-x)PZT-xBFO samples sintered at 950°C/2 h

This results in the grains being very tightly packed which reduces the porosity. The average grain size is presented in Table 2 and Figure 6. It can be seen that the evolution of grain size is not linear, it increases with the increase of BFO content until x= 0.30 then it decreases for x= 0.60. The large grain size was attributed, according to C. Chen and al [34], to the high KOH concentration (between 6 M and 10 M) and high hydrothermal treatment temperature (200°C). These morphological changes can lead to a variation in the ferroelectric and magnetic response of these composites.
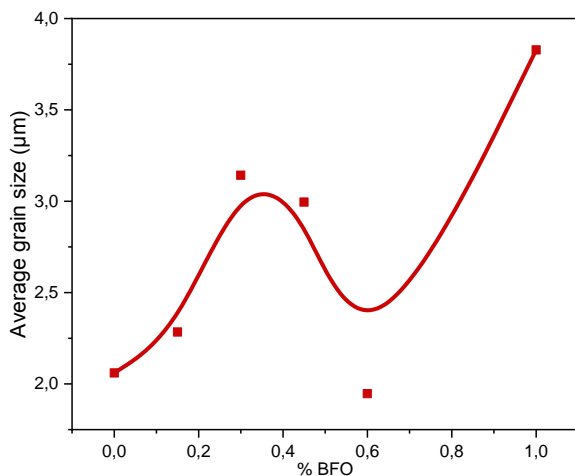

Fig. 6. Average grain size of samples (1-x)PZT-xBFO

To confirm the presence of the elemental components (Pb, Zr, Ti, Bi, Fe, and O) in (1-x)PZT-xBFO ceramics, we used X-ray energy dispersive spectroscopy (EDS). This technique is based on the energy of photons emitted when an electron de-excites from an outer level to a deep level. The photon is then analyzed and counted according to its energy. This energy is characteristic of an electronic transition, i.e. a given chemical species. The results are shown in Figure 7 and Table 3. The EDS spectra of our

pellets show that all the characteristic lines of the chemical elements Pb, Zr, Ti, and O and Bi, Fe, and O are present for PZT and BFO respectively. While for the composites, we observe that Bi was not identified on the surface of the ceramics, it is also the case for Zr and Pb which were not detected for x= 0.45 and x= 0.60 respectively. The absence of these elements is attributed to the evolution of the intensity of the main peaks of Pb and Bi in the energy range of 2 to 3 KeV, which prevents the possibility of clearly observing the change in intensity of these peaks forming the (1-x)PZT-xBFO samples are presented in Table 3, (where for some compositions the percentage is less than 100%).

3.4. Dielectric Studies

Figure 8 shows the evolution of the relative dielectric constant of the (1-x)PZT-xBFO samples with x= 0.00, 0.15, 0.30, 0.45, 0.60, and 1.00 as a function of temperature at different frequencies. It is observed that BFO has an important role in the dielectric response of PZT. However, for pure PZT relative dielectric constant increases gradually with increasing temperature and reaches a maximum value of ε_{max}(=1391 at 2 MHz) at 420°C for all frequencies. This dielectric anomaly indicates a classical phase transition from ferroelectric to paraelectric phase. The same behavior was found by S. Sharma and al for 0.95 PZT-0.05 BFO compound [44]. When BFO is added to PZT at different concentrations, the evolution as a function of temperature shows two different behaviors compared to pure PZT. At frequencies <1 MHz, a similar behavior as pure PZT is obtained and the transition temperature decreases for x= 0.15 and then increases until x= 0.40. We can also notice that the peak of this anomaly becomes diffuse which confirms the diffuse behavior of these ceramics.

Table 2. Average grain size of (1-x)PZT-xBFO ceramics

% BFO	x= 0.00	x= 0.15	x= 0.30	x= 0.45	x= 0.60	x= 1.00
Average grain size (µm)	2.060	2.284	3.1425	2.9954	1.9465	3.828

Table 3. Mole fraction of elements Pb, Zr, Ti, Bi, Fe, and O obtained by EDS analysis

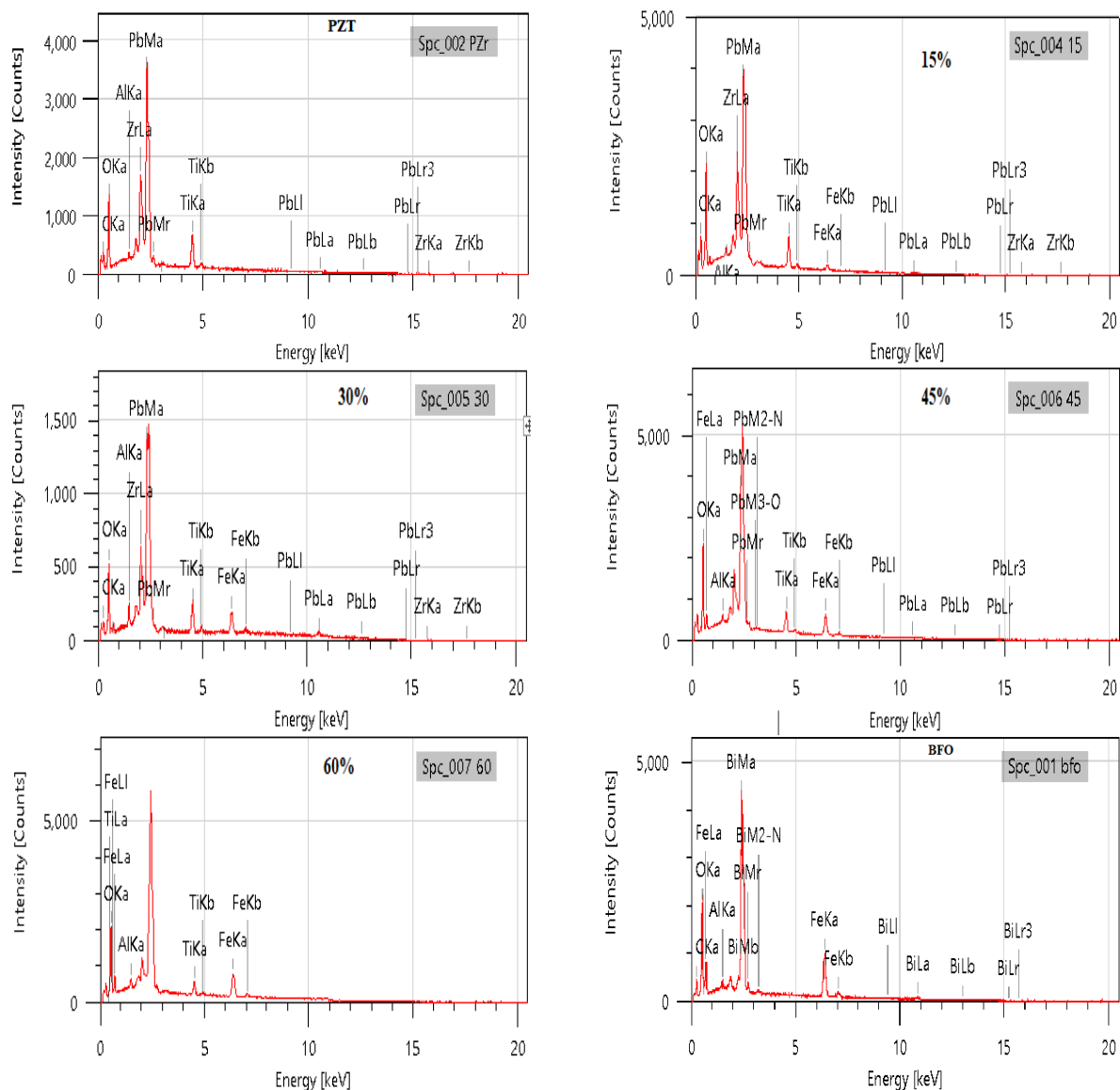| Elément	x= 0.00	x= 0.15	x= 0.30	x= 0.45	x= 0.60	x= 1.00
Pb	0.5912	0.4852	0.4944			
Zr	0.1444	0.1593	0.1301	0.4666	0.1165	
Ti	0.795	0.660	0.787			
Bi				0.828	0.5142	0.6105
Fe		0.238	0.1113	0.1808		0.2206
O	0.1526	0.2009	0.1474	0.2609	0.3454	0.1418

Fig. 7. EDS analysis of (1-x)PZT-xBFO ceramics sintered at 950°C (2 h)

Beyond this value (x= 0.40), the temperature transition shifts to lower values as the value of x varies from 0.40 to 1.00 (Table 4). In addition, the value of ε_{max} increases with increasing BFO content in (1-x)PZT-xBFO compounds up to x= 0.45 followed by a decrease for x= 0.60. The increase in the value of the relative dielectric constant can be attributed to the electron-photon interaction [36]. S.H. Jo et al [5] reported that good dielectric properties are achieved for PZT/BFO samples due to the rhombohedral crystal structure distortion of BFO related to the large ionic displacements in the distorted perovskite structure. On the other hand, for frequencies above 1 MHz, the value of ε_{max} increases with increasing temperature and reaches a maximum peak (ε_{max}) at frequency-dependent temperature T_m. Indeed, the value of T_m shifts to lower temperatures as the frequency increases accompanied by a decrease of ε_{max} value. Above maximal temperature Tm, the value of the maximum relative dielectric constant decreases sharply to a minimum value at a particular temperature and then increases. This phenomenon is attributed to dielectric resonance [28, 29, 45]. The peak associated with this resonance becomes increasingly diffuse as the BFO content increases. For x= 0.15, we observe a second anomaly at a second temperature T_m for the frequencies 1 MHz, 1.4 MHz, and 2 MHz. This anomaly is due to the symmetry of resonance and antiresonance frequency for the minimum temperature.

8

However, further investigation and discussion are necessary to understand these new phenomena that we found for the first time for PZT/BFO hybrid composites.
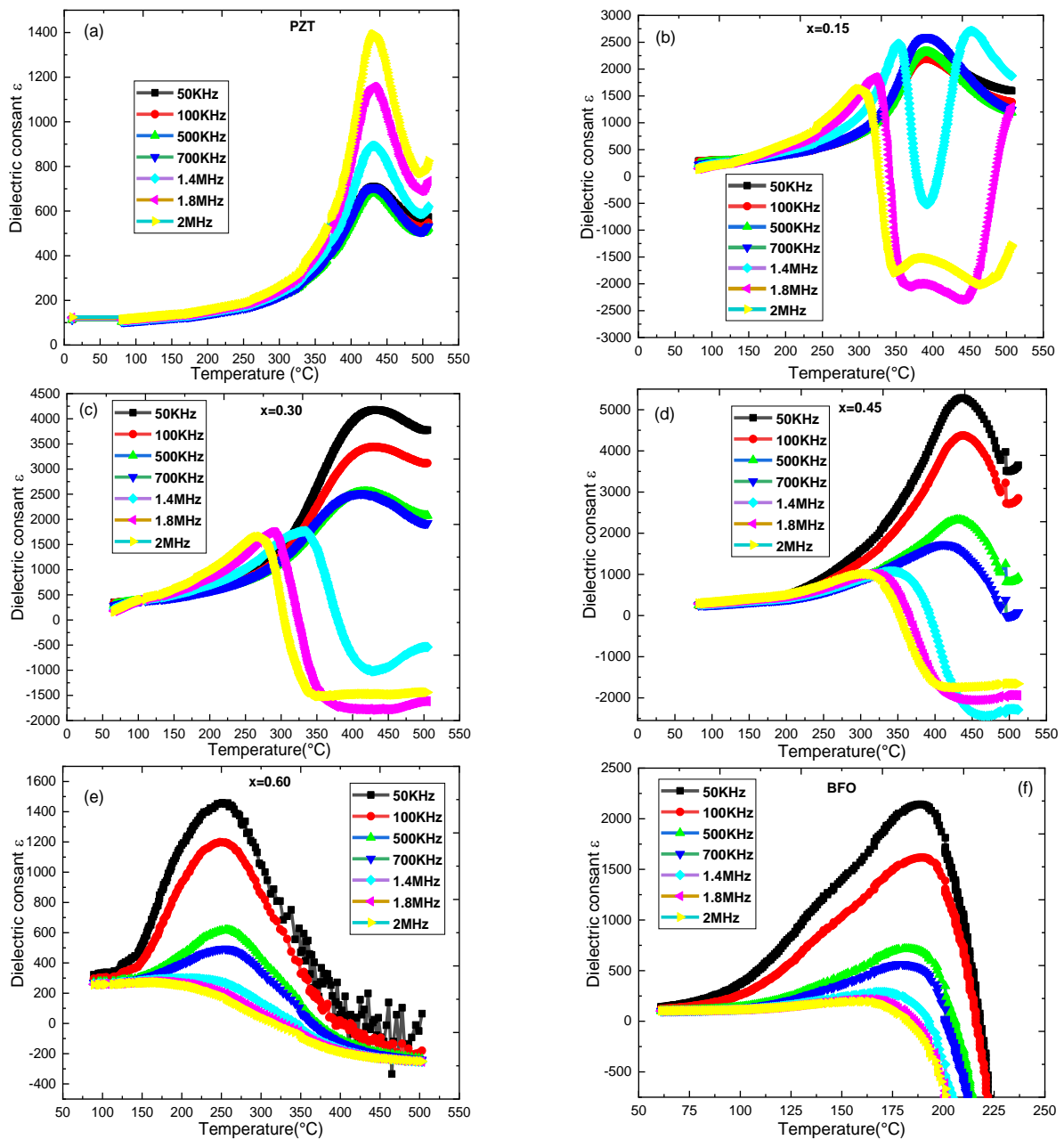
Fig. 8. Evolution of dielectric permittivity of sintered (1-x)PZT-xBFO composites at 950°C/2 h as a function of temperature at different frequencies

Table 4. Values of Tm and ε_{rmax} at different frequencies of (1-x)PZT-xBFO composites

x	100 KHz		1.4 MHz		2 MHz	
	T_m	ε_m	T_m	ε_m	T_m	ε_m
x= 0.00	432	700	432	912	432	1405
x= 0.15	388	2251	353	2529	296	1694
x= 0.30	423	3511	326	1853	262	1752
x= 0.45	434	4463	334	1161	291	1381
x= 0.60	244	1221	210	304	164	282
x= 1.00	189	1653	166	321	160	233

Figure 9 shows the variation of dielectric losses (tanδ) as a function of temperature at frequencies ranging from 50 kHz to 2 MHz. For x= 0.00, the dielectric loss increases slightly up to 300°C, then increases significantly with temperature until it reaches a maximum value. The position and losses depend on the frequency. For x>0, the dielectric losses are almost constant and almost zero but show sharp peaks. These peaks move towards lower temperatures as the frequency increases. It can also be seen that the

values of the dielectric losses decrease with the addition of BFO to the PZT ceramic for x= 0.30 and increase for the other values of x. The increase in dielectric losses may be due to relaxation at low frequencies or to the diffusion of charge carriers.

It was also noted that as the BFO content increased, so did the dielectric loss values compared with pure PZT, highlighting the fact that electrical conduction becomes increasingly important as the temperature rises (Fe^{2+}---$Fe^{3+}+e^{-}$).
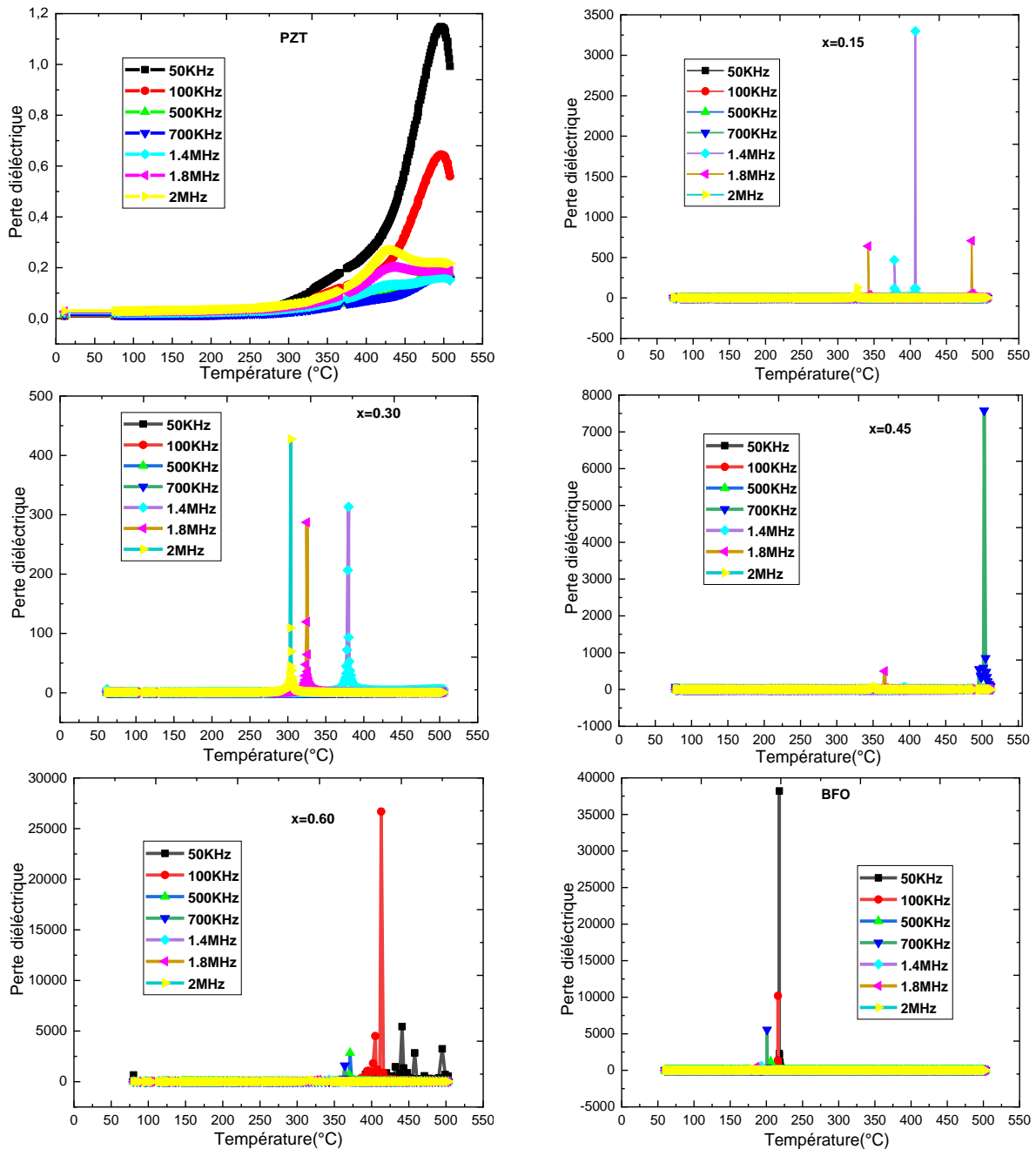

Fig. 9. Temperature dependence of dielectric losses of (1-x)PZT-xBFO ceramics for $0 \leq x \leq 1$

4. CONCLUSIONS

In summary, structural, microstructural, and dielectric properties of all the compounds in the system (1-x)BFO-xPZT (x= 0.00, 0.15, 0.30, 0.45, 0.60, and 1.00) were carried out. Rietveld study of structural properties suggested the coexistence of three phases: rhombohedral, tetragonal of PZT, and rhombohedral for BFO. The Raman spectra of (1-x)BFO-xPZT ceramics showed that the intensity of bands Raman is much lower than for pure BFO and the intensity of the A1(2TO) mode increases from x= 0.0 to x= 0.45 and then decreased. The SEM results showed that, as the BFO increased in size, the grains in the BFO sample were larger than those in the other composites and in the pure PZT. These agglomerates formed huge, complex clusters. The dielectric behavior indicated a resonance phenomenon for all the composites and the symmetric resonance-antiresonance was found for x= 0.15 at a high frequency range. Also, the dielectric permittivity value improved with BFO addition compared with pure PZT.

REFERENCES

[1]. A. Gupta and R. Chatterjee, "Study of dielectric and magnetic properties of $PbZr_{0.52}Ti_{0.48}O_3$-$Mn_{0.3}Co_{0.6}Zn_{0.4}Fe_{1.7}O_4$ composite". J. Magn. Magn. Mater., 2010, vol. 322, no. 8, pp. 1020–1025, doi: 10.1016/j.jmmm.2009.12.007.

[2]. M. Hordagoda., Growth, characterization, and function of ferroelectric, ferromagnetic thin films and their heterostructures, University of South Florida, 2017.

[3]. T. Zhao et al., "Electrical control of antiferromagnetic domains in multiferroic $BiFeO_3$ films at room temperature". Nat. Mater., 2006, vol. 5, no. 10, pp. 823–829, doi: 10.1038/nmat1731.

[4]. Y. Yamasaki, S. Miyasaka, Y. Kaneko, J. P. He, T. Arima, and Y. Tokura, "Magnetic reversal of the ferroelectric polarization in a multiferroic spinel oxide". Phys. Rev. Lett., 2006, vol. 96, no. 20, pp. 1–4, doi: 10.1103/PhysRevLett.96.207204.

[5]. S. H. Jo, S. G. Lee, and Y. H. Lee, "Ferroelectric properties of PZT/BFO multilayer thin films prepared using the sol-gel method". Nanoscale Res. Lett., 2012, vol. 7, no. 3, pp. 4–8, doi: 10.1186/1556-276X-7-54.

[6]. M. Bibes and A. Barthélémy, "Multiferroics: Towards a magnetoelectric memory". Nat. Mater., 2008, vol. 7, no. 6, pp. 425–426, doi: 10.1038/nmat2189.

[7]. F. Yan et al., "Role of $Pb(Zr_{0.52}Ti_{0.48})O_3$ substitution in multiferroic properties of polycrystalline $BiFeO_3$ thin films", J. Appl. Phys, 2011, vol. 114116, pp. 0–6, doi: 10.1063/1.3668123.

[8]. Y. W. Li, J. L. Sun, J. Chen, X. J. Meng, and J. H. Chu, "Structural, ferroelectric, dielectric, and magnetic properties of $BiFeO_3$/$Pb(Zr_{0.5}Ti_{0.5})O_3$ multilayer films derived by chemical solution deposition", Appl. Phys. Lett., 2005, vol. 87, no. 18, pp. 1–3, doi: 10.1063/1.2120907.

[9]. A. P. Singh, "Synthesis and Characterization of Bismuth Ferrite and Lead Zirconium Titanate (BFO-PZT) Laminate Composite," Thapar University, Patiala.

[10]. X. He et al., "Dielectric performance controlled by magnetic field in PZT-BFO gradient multiferroic ceramics," Ferroelectrics, 2017, vol. 514, no. 1, pp. 158–164, doi: 10.1080/00150193.2017.1357989.

[11]. X. Y. Zhang, X. W. Qi, Z. Y. Yang, and R. X. Zhong, "Comparative studies of multiferroic $BiFeO_3$ powders prepared by hydrothermal method versus sol-gel process," Appl. Mech. Mater., vol. 670–671, no. 3, pp. 113–116, 2014, doi: 10.4028/www.scientific.net/AMM.670-671.113.

[12]. A. V. Egorysheva et al., "Synthesis of high-purity nanocrystalline $BiFeO_3$," Inorg. Mater., 2013, vol. 49, no. 3, pp. 310–314, doi: 10.1134/S0020168513030035.

[13]. S. Sharma, V. Singh, R. K. Kotnala, and R. K. Dwivedi, "Comparative studies of pure BiFeO3 prepared by sol-gel versus conventional solid-state-reaction method," J. Mater. Sci. Mater. Electron., 2014, vol. 25, no. 4, pp. 1915–1921, doi: 10.1007/s10854-014-1820-7.

[14]. S. H. Han et al., "Synthesis and characterization of multiferroic $BiFeO_3$ powders fabricated by hydrothermal method," Ceram. Int., 2010, vol. 36, no. 4, pp. 1365–1372, doi:

10.1016/j.ceramint.2010.01.020.

[15]. A. V. Egorysheva et al., "Mechanochemical activation of starting oxide mixtures for solid-state synthesis of BiFeO$_3$," Inorg. Mater., 2013, vol. 49, no. 3, pp. 303–309, doi: 10.1134/S0020168513030023.

[16]. M. S. Bernardo, T. Jardiel, M. Peiteado, A. C. Caballero, and M. Villegas, "Reaction pathways in the solid state synthesis of multiferroic BiFeO$_3$," J. Eur. Ceram. Soc., 2011, vol. 31, no. 16, pp. 3047–3053, doi: 10.1016/j.jeurceramsoc.2011.03.018.

[17]. M. Zimmerman, N. A. Peterson, and M. A. Zimmerman, "Beyond the Individual : Toward a Nomological Network of Organizational Empowerment Beyond the Individual : Toward a Nomological Network of Organizational Empowerment," American Journal of Community Psychology, 2004, Volume 34, Issue 1-2, Pages 129-145.

[18]. Q. Yang, Y. Li, Q. Yin, P. Wang, and Y. B. Cheng, "Hydrothermal synthesis of bismuth oxide needles," Mater. Lett., 2002, vol. 55, no. 1–2, pp. 46–49, doi: 10.1016/S0167-577X(01)00617-6.

[19]. M. Muneeswaran, P. Jegatheesan, and N. V. Giridharan, "Synthesis of nanosized BiFeO$_3$ powders by co-precipitation method," J. Exp. Nanosci., 2013, vol. 8, no. 3, pp. 341–346, doi: 10.1080/17458080.2012.685954.

[20]. L. Jin, "Broadband Dielectric Response in Hard and Soft PZT : Understanding Softening and Hardening Mechanisms," 2011, vol. 4988.

[21]. B. Noheda, J. Gonzalo, L. Cross, R. Guo, and S. Park, "Tetragonal-to-monoclinic phase transition in a ferroelectric perovskite: The structure of PbZr$_{0.52}$Ti$_{0.48}$O$_3$," Phys. Rev. B-Condens. Matter Mater. Phys., 2000, vol. 61, no. 13, pp. 8687–8695, doi: 10.1103/PhysRevB.61.8687.

[22]. S. Nayak, T. Kumar, and D. Khastgir, "permittivity : Switchable dielectric phase transition with temperature," Ceram. Int., 2016, vol. 42, no. 13, pp. 14490–14498, doi: 10.1016/j.ceramint.2016.06.056.

[23]. S. H. Jo, S. P. Nam, S. G. Lee, S. H. Lee, Y. H. Lee, and Y. G. Kim, "Fabrication and electrical properties of PZT/BFO multilayer thin films," Trans. Electr. Electron. Mater., 2011, vol. 12, no. 5, pp. 193–196, doi: 10.4313/TEEM.2011.12.5.193.

[24]. M. Mehak et al., "Multiferroic triphase BFO-PZT-PVDF composite with significant magnetoelectric response for multistate device applications," Ceram. Int., 2021, Vol. 47, no. 15, pp. 21688–21697, doi: 10.1016/j.ceramint.2021.04.182.

[25]. S. Sharma and R. K. Dwivedi, "Substitutionally driven phase transition and enhanced multiferroic and electrical properties of $(1−x)$BiFeO$_3$–(x)Pb(Zr$_{0.52}$Ti$_{0.48}$)O$_3$ ceramics ($0.0 \leq x \leq 1.00$)," J. Alloys Compd., 2017, vol. 692, pp. 770–773, doi: 10.1016/j.jallcom.2016.09.067.

[26]. S. Sharma, V. Singh, R. K. Kotnala, R. Ranjan, and R. K. Dwivedi, "Co-existence of tetragonal and monoclinic phases and multiferroic properties for $x \leq 0.30$ in the $(1-x)$Pb(Zr$_{0.52}$Ti$_{0.48}$)O$_3$-(x)BiFeO$_3$ system," J. Alloys Compd., 2014, vol. 614, pp. 165–172, doi: 10.1016/j.jallcom.2014.06.061.

[27]. C. Yan, X. Liu, H. Sun, H. Sui, and Y. Wang, "Enhanced ferroelectric and dielectric behaviors of PZT/BFO heterostructure via compositional development," J. Mater. Sci. Mater. Electron., 2021, vol. 32, no. 7, pp. 8185–8194, doi:10.1007/s10854-020-050249.

[28]. M. Ahabboud, M. Amarass, A. F. Abdi, and T. Lamcharfi, "Structural and dielectric properties of Pb(Zr$_{0.52}$Ti$_{0.48}$)$_{1-3x}$/4Fe$_x$O$_3$ ceramics at $0 \leq x \leq 0.20$ prepared by sol-gel method," IOP Conf. Ser. Mater. Sci. Eng., 2021, pp. 1–3, doi: 10.1088/1757-899X/1160/1/012001.

[29]. M. Ahabboud, T. Lamcharfi, F. Abdi, N. Hadi, F. Z. Ajyaje, and M. Haddad, "Effect of Cu Doping on Structural and Dielectric Properties of Pb$_{1-x}$Cu$_x$(Zr$_{0.52}$Ti$_{0.48}$)O$_3$ (PCx ZT) ($0 \leq x \leq 0.2$) Ceramics Prepared by Sol-Gel Method M." Asian J. Chem., 2018 vol. 30, no. 18, pp. 2424–2430.

[30]. J. Wei, C. Zhang, and Z. Xu, "Low-temperature hydrothermal synthesis of BiFeO$_3$ microcrystals and their visible-light photocatalytic activity," Mater. Res. Bull., 2012, vol. 47, no. 11, pp. 3513–3517, doi: 10.1016/j.materresbull.2012.06.068.

[31]. H. Jiang, Y. Morozumi, N. Kumada, Y.

12

Yonesaki, T. Takei, and N. Kinomura, "Hydrothermal synthesis of perovskite-type BiFeO₃," J. Ceram. Soc. Japan, 2008, vol. 116, no. 1355, pp. 837–839, doi: 10.2109/jcersj2.116.837.

[32]. A. Malika, G. Najwa, F. Z. Ahjyaje, L. Taj-Dine, and A. Farid, "Resonance phenomenon and structural properties of fe substituted PZT ceramics prepared by the sol-gel method," Iran. J. Mater. Sci. Eng., 2023, vol. 20, no. 1, pp. 1–14, doi: 10.22068/ijmse.2938.

[33]. P. Kour, S. K. Pradhan, P. Kumar, S. K. Sinha, and M. Kar, "Enhanced ferroeletric and piezoelectric properties of Nd³⁺ doped PZT nanoceramics", AIP Conf. Proc., 2016, Vol. 1728, pp. 3–7, doi: 10.1063/1.4946541.

[34]. C. Chen, J. Cheng, S. Yu, L. Che, and Z. Meng, "Hydrothermal synthesis of perovskite bismuth ferrite crystallites", J. Cryst. Growth, 2006, vol. 291, no. 1, pp. 135–139, doi: 10.1016/j.jcrysgro.2006.02.048.

[35]. M. Atif, M. Nadeem, R. Grossinger, R. S. Turtelli, and F.Kubel, "Magnetic, dielectric and magnetoelectric properties in $(1-x)Pb(Zr_{0.52}Ti_{0.48})O_3$ + $(x)CoFe_2O_4$ composites," J Mater Sci Mater Electron other, 2015, doi: 10.1007/s10854-015-3418-0.

[36]. S. Sharma, "Rietveld analysis, magnetic, transport, and optical properties of $(1-x)BiFeO_3-(x)Pb(Zr_{0.52}Ti_{0.48})O_3$ ceramics prepared by sol-gel route," J. Mater. Sci. Mater. Electron., 2020, vol. 31, no. 10, pp. 7776–7785, doi: 10.1007/s10854-020-03316-8.

[37]. C. P. Bhole, "Antiferromagnetic to paramagnetic phase transitions in bismuth ferrite (BiFeO₃) ceramics by solid-state reaction," Ceram. -Silikaty, 2012, vol. 56, no. 2, pp. 127–129.

[38]. J. Rouquette, J. Haines, V. Bornand, M. Pintard, and P. Papet, "Transition to a cubic phase with symmetry-breaking disorder in $PbZr_{0.52}Ti_{0.48}O_3$ at high pressure," Phys. Rev. B, 2002, vol. 65, pp. 1–4, doi: 10.1103/PhysRevB.65.214102.

[39]. E. Buixaderas, M. Berta, L. Kozielski, and I. Gregora, "Raman spectroscopy of $Pb(Zr_{1-x}Ti_x)O_3$ graded ceramics around the morphotropic phase boundary," Phase Transitions, no. 2013, pp. 37–41, doi: 10.1080/01411594.2011.552049.

[40]. S. Samanta, M. Muralidhar, V. Sankaranarayanan, K. Sethupathi, M. S. R. Rao, and M. Murakami, "Band gap reduction and redshift of lattice vibrational spectra in Nb and Fe co-doped PLZT," J. Mater. Sci., 2017, doi: 10.1007/s10853-017-1425-7.

[41]. S. Sharma, V. Singh, R. K. Dwivedi, R. Ranjan, A. Anshul, and S. S. Amritphale, "Phase transformation, improved ferroelectric and magnetic properties of $(1x)BiFeO_3-xPb(Zr_{0.52}Ti_{0.48})O_3$ solid solutions Subhash," J. Appl. Phys., 2014, vol. 224106, pp. 0–7, doi: 10.1063/1.4882067.

[42]. H. Fukumura, H. Harima, K. Kisoda, M. Tamada, Y. Noguchi, and M. Miyayama, "Raman scattering study of multiferroic BiFeO₃ single crystal," J. Magn. Magn. Mater., 2007, vol. 310, no. 2 SUPPL. PART 2, pp. 2006–2008, doi: 10.1016/j.jmmm.2006.10.282.

[43]. P. Pandit, S. Satapathy, P. K. Gupta, and V. G. Sathe, "Effect of coalesce doping of Nd and la on structure, dielectric, and magnetic properties of BiFeO₃," J. Appl. Phys., 2009, vol. 106, no. 11, pp. 3–10, doi: 10.1063/1.3264836.

[44]. S. Sharma, V. Singh, O. Parkash, and R. K. Dwivedi, "Effect of processing on dielectric properties of $(0.95)PbZr_{0.52}Ti_{0.48}O_3$-$(0.05)BiFeO_3$," Appl. Phys. A Mater. Sci. Process., 2013, vol. 112, no. 4, pp. 975–984, doi: 10.1007/s00339-012-7458-5.

[45]. R. A. Cowley, S. N. Gvasaliya, S. G. Lushnikov, B. Roessli, and G. M. Rotaru, "Relaxing with relaxors: A review of relaxor ferroelectrics," Adv. Phys., 2011, vol. 60, no. 2, pp. 229–327, doi: 10.1080/00018732.2011.555385.

[46]. N. Panda, S. Pattanayak, R. N. P. Choudhary, and A. Kumar, "Effect of La-substitution on structural, dielectric and electrical properties of $(Bi_{0.5}Pb_{0.5})(Fe_{0.5}Zr_{0.25}Ti_{0.25})O_3$," Appl. Phys. A Mater. Sci. Process., 2016, vol. 122, no. 9, doi: 10.1007/s00339-016-0321-3.